Gold surface cleaning by etching polishing: optimization of polycrystalline film topography and surface functionality for biosensing

Borys Snopok[1,2,3,*], Arwa Laroussi[2,5], Clodomiro Cafolla[4], Kislon Voïtchovsky[3,4], Tetyana Snopok[1], Vladimir M.Mirsky[2]

[1] VE Lashkaryov Institute of semiconductor physics, NAS of Ukraine, Kyiv, Ukraine
[2] Nanobiotechnology - Institute of Biotechnology, Brandenburg Technical University, Cottbus-Senftenberg, Germany
[3] Durham University, Institute of Advanced Study, Durham DH1 3LE, UK
[4] Durham University, Physics Department, Durham DH1 3LE, UK
[5] University of Tunis El-Manar, Faculty of Science of Tunis, Chemistry Department, Laboratory of Analytical Chemistry and Electrochemistry (LR99ES15), 2092 Tunis El-Manar, Tunisia

*corresponding author, email: snopok@isp.kiev.ua

Abstract
Modern bio-chemical sensors rely on functional interfacial architectures with well-defined structural nano-motifs over a physical transducer. Gold-coated interfaces are of particular interest for their desirable chemical (functionalization) and optical (plasmonic) properties. Here we investigate the cleaning and polishing of polycrystalline gold films in preparation of advanced surface functionalization. We focus on soft wet chemical etching to decrease the small-scale roughness commonly observed after evaporation or sputtering of gold. We show that optimized surfaces are obtained by etching in solutions of hydrochloric acid and hydrogen peroxide. We systematically quantify the films wettability, surface nano-topography, UV-VIS spectrum and the electrochemical and Surface Plasmon Resonance (SPR) changes throughout the etching process. Optimal results are obtained by etching with a HCl(37%):H_2O_2(30%):H_2O mixture, with a volume ratio of reagents 3:3:94 during 15-20 minutes at room temperature for the main step. This reduces by a factor two the root-mean-square roughness, removes contaminants, increases hydrophilicity and modifies the gold surface by $Au(Cl)_x$ complexes. Significantly, the resulting the surface is hydrophilic enough to prevent globular proteins such as HSA to unfold upon deposition at concentrations more than ~1 mg/mL. Our protocol offers a simple, reliable and rapid method for the preparation of gold surface in view of further functionalization including the binding of receptor layers and various micro- and nanostructures required in chemical and biochemical sensing.

Keywords polycrystalline gold films, soft wet chemical polishing, gold cleaning, hydrochloric acid and hydrogen peroxide, protein adsorption, surface plasmon resonance

1. Introduction

Molecule-specific bio-chemical sensors often rely on a functionalized sensing layer that can capture target molecules. The recognition efficiency of a given receptor site dictates the sensor functionality and the sensing layer is therefore crucial for the sensor performance [1-3]. This is particularly important for affine biosensors where preservation of the receptor molecules imposes strict constraints of the interfacial architecture [4-5]. Currently, the main biosensing approaches involve the integration of nano-sized building blocks such as functionalized nanoparticles, biological macromolecules or conjugates of nanoparticles with bio-recognition sites with surface-based physical transducers. This strategy requires careful control of the interfacial architecture, as illustrated by sensors relying on functionalized gold surfaces: a thin gold film supports a self-assembled monolayers (SAM) of thiols which itself acts as an intermediate layer for the coupling of a wide range of functional biomolecules [6-8]. While flexible and powerful, this strategy fails for rough gold substrates; studies have established a correlation between the substrate roughness and the density of defects in SAMs as well as the stability of the monolayer systems itself [9, 10]. Moreover, topographic and chemical singularities in the sensor surface can destroy the native conformation of biomolecules and preclude deposition of interfacial architectures [11, 12]. To overcome these issues, it is crucial for the native gold surface to undergo (i) removal of contaminants, (ii) optimal smoothing and (iii) task-specific surface 'passivation' by weakly bounded anions. Indeed, while it is still possible to make a poor coating on an excellent substrate, the inverse is not true, emphasizing the need for a thorough and optimized preparation of the substrate. This pre-treatment must be cheap, easily integrated into conventional production process and reproducible to enable a consistently high functionalization quality and hence sensor reliability.

Aside from the requirements imposed by the sensor functionalization, the detection mechanism also needs to be considered. Gold-based biosensors are widely used for Surface Plasmon Resonance (SPR) measurements which are particularly sensitive to surface imperfections in the gold. This is due to scattering of the captured light and a complex interplay between signal measured and the functionalizing elements of the sensor [1, 5, 7, 13]. Surface roughness leads to broadening of the resonance spectra and increases the background noise [14-16]. Yet, conventional SPR chips rely on inexpensive polycrystalline gold films with relatively high roughness [17, 18]. SPR detection therefore also requires optimization of the transducer's surface topography and chemical reactivity. Considering the nanoscale size of typical functional units, the narrow linear range of SPR transducers and the need to decrease both elastic and inelastic scattering of surface plasmons, optimization must take place at the nanoscale [5, 11, 19-21].

A wide variety of approaches have been proposed to control the nanoscale topography and chemical reactivity of polycrystalline gold films [22-24], but no single process meets all the technical requirements. Physical treatments such as inert [9, 10, 16, 30] or reactive annealing in hydrogen sulfide atmosphere [31], plasma discharge treatment [32, 33] and other similar techniques [34-36] can desorb or decompose loosely coupled substances. However, heat treatment does not exclude subsequent contamination by strongly binding molecules and is hence not ideal where high purity or biochemical modification is required. In contrast, chemical cleaning such as electrochemical polishing [37-39] and dissolution of contamination by common solvents and detergents suffer from the risk of damaging the adhesive chromium layer [40, 41]. The widely spread use of hydrogen peroxide (so-called Piranha solution made of a 3:1 v/v mixture of hydrogen peroxide and sulfuric acid) can remove nearly all organics [42], but often leads to extensive and uncontrolled etching of the surface [43]. Alternatively, peroxydisulfate offers an aqueous-based technology for the oxidative destruction of the organic components [44], using sodium or ammonium peroxydisulfate to turn organic material into

carbon dioxide and water [45]. Acid-based cleaners tend to create additional surface heterogeneity on polycrystalline gold films and leave behind weakly adhesive interfacial contaminants [46] that require an additional so called 'soft etching' step. Soft etching refers to both the dissolution of the metal and the passivation its surface using anions that can form gold complexes [50]. Mixtures of non-oxidizing hydrochloric acid and hydrogen peroxide have a softer impact on thin gold films and provide suitable surfaces for SPR techniques [25-29, 51-54]: hydrogen peroxide oxidizes the gold surface while chloride ions form soluble complexes dissolving the gold layer. Finally, it is worth mentioning the so-called RCA (ascribed to Werner Kern at RCA Laboratories, Princeton) treatment routinely used in the microelectronic industry [56]. The RCA approach is a two-stage process based on an aqueous mixture of hydrogen peroxide, ammonia followed by an aqueous mixture of hydrogen peroxide with hydrochloric acid (HCl), with many existing variations for the first step [57].
Generally, treatments with low concentrated water solution of hydrochloric acid and hydrogen peroxide (HAHP) can remove particulates and reduce the surface roughness [25-29]. This method is attractive for its ease of use but there is no clear recipe for achieving reliable treatment conditions with surface transformations spanning from the nano- to macro-scale. This is precisely the goal of this paper which establishes a clear procedure for reproducibly achieving optimized gold surfaces suitable for functionalization and SPR measurements.

2. Materials and methods

2.1 Chemicals and Reagents

Chemical (hydrochloric acid (HCl, 37%), hydrogen peroxide (H_2O_2, 30%), H_2SO_4 (37%), acetone, ethanol, isopropanol, NaCl, glycine, distilled water) and biochemical (HSA (Sigma A1653, albumin from human serum), rabbit polyclonal anti-human albumin antibody (Sigma A0433)) reagents were purchased from Sigma-Aldrich. All buffers (PBS (pH 7.4)) and regeneration solutions were prepared according to the standard procedures using Milli-Q-purified water.
1 mg/ml HSA in PBS (pH 7.4) was used as a stock solution. The solution of anti-HSA antibody was aliquoted in PBS (pH 7.4) (50 µl) and stored at -20°C. Working solutions of anti-HSA (50 µl in 2 ml PBS) were prepared from the stock solution immediately before conducting measurements.

2.2 Gold films fabrication

The SPR chip support was made of a glass plate (TF4, refractive index n = 1.61) with dimensions of 20×20×1 mm^3. For the film fabrication, the upper side of the plate was covered with a ~5 nm adhesive layer of chromium followed by a 50±3 nm of gold using thermal evaporation of gold wires in vacuum (the system VUP-5M was used, the evaporation rate c.a. 4-5 nm/s). The mass thickness of the films during deposition was controlled using a calibrated QCM sensor and sample-inspect by ellipsometric measurements (LEF-3M ellipsometer). During the deposition, the plate was kept at 22°C, and then for three hours in high vacuum (5×10^{-4} Pa) before removal from the evaporation equipment for soft relaxation of the mechanical stresses within the film.

2.3 Rinsing off by organic solvents

To remove loosely adhesive contaminations, an intensive rinsing with consecutively acetone, ethanol, isopropanol, and distilled water was carried out. The substrates were fixed on a mount

and washed under a stream of solvent from laboratory wash bottles in a direction tangential to the surface. After rinsing, the remaining water was removed with a stream of dried argon, directed tangentially to the surface. Alternatively, the substrates were placed in a container filled with distilled water until the next treatment procedure.

2.4 Piranha cleaning protocol

The Piranha solution used had a composition of 1 volume of H_2O_2 (30%) to 3 volumes of concentrated H_2SO_4 (37%). The samples were slowly immersed in a solution of freshly prepared Piranha etch and incubated for 20-60 s (Caution! Exothermal reaction!). After the treatment, the substrate was washed in distilled water under a stream and by stored in pure water. The Piranha solution was freshly prepared to minimize the self-decomposition of H_2O_2. It is also advisable to immerse the substrate into the solution slowly in order to prevent thermal shock of thin gold films. The procedure assumes that large amount of organic impurities have been previously washed off the surface.

2.5 Etching-polishing protocol

For the preparation of the HAHP etching solution (x) aliquots of hydrochloric acid (HCl, 37%) and (x) aliquots of hydrogen peroxide (H_2O_2, 30%) were dissolved in (100-2x) parts of distilled water in the volumetric mixing ratio (x)HCl:(x)H_2O_2:(100-2x)H_2O (v/v/v), $x \in [0, 7]$. During the etching, the sample was kept at T = 21±1°C. Each cleaning procedure was applied to several samples to obtain statistically meaningful results. Optimization of the condition for the soft etching-polishing step (5-25 min immersion for polycrystalline gold films) were performed using $x \in [0, 7]$. For x>7, oxygen bubbles were generated on the surface during the etching process. The bubbles can create local variations in the concentration of active components at the surface and lead to a non-uniform etching.

2.6 Characterization methods

2.6.1 Surface analysis: Atomic Force Microscopy (AFM)

Nanoscale surface characterization of the samples' topography was performed with a commercial Cypher ES atomic force microscope (Oxford Instruments, Santa Barbara, CA, USA), equipped with a temperature control system. Imaging was conducted in pure water using back-coated silicon nitride probes (Arrow UHF, Nanoworld, Switzerland). Each cantilever was calibrated using its thermal spectrum [61] and found to have typical stiffness of 2 (± 0.5) Nm^{-1}. The AFM was operated in amplitude modulation using cantilevers oscillated close to their fundamental resonance (~400 kHz in water). The imaging was carried out with the highest possible setpoint ratio (typically >0.9). In amplitude modulation, the topographic images represent the vertical corrections applied by the feedback loop to maintain the tip vibration amplitude constant as it scans the surface of the sample. The phase lag between the driving and the measured oscillations can vary freely and is recorded. When operated in water and with small oscillations amplitudes (<1-2 nm) the phase is sensitive to the local wetting properties of the surface as experienced by the imaging tip [62]. Images were stored as 256×256 matrices of pixels with topography, amplitude and phase acquired simultaneously.

The measurements were conducted at 25°C after achieving thermal equilibrium. Imaging analysis was performed using Gwyddion Software [63] and bespoke routines programmed in Igor Pro (Wavemetrics, Lake Oswego, OR, USA).

2.6.2 Contact angle measurement

Statics water contact angles were measured by a computer-controlled Pendant Drop CAM 200 device (KSV Instruments Ltd, Helsinki, Finland) assembled on a vibrationally isolated platform. The measurements were performed in atmospheric environment at 20 °C. For each measurement, a 5 μL droplet of MilliQ water was put on the film using a micro syringe, and the image of the droplet was automatically taken as a function of time. A CCD camera (512×480) with telecentric lens combined with a LED-based background red lighting was used for capturing images at 1-10 fps. From these images, contact angle values were calculated with dedicated software using complete curve (droplet profile) fitting based on a Laplace-Young equation (CAM 2008 software, KSV CAM Optical Contact Angle (v.4.01), KSV Instruments Ltd, Helsinki, Finland). All reported contact angles are the average of at least three measurements taken at different locations on the same substrate and have a maximum error of 3°.

2.6.3 Optical Measurements

The UV-VIS spectra of samples were recorded using an Evolution 220 spectrometer (Thermo Scientific, Germany). The spectra were collected in the absorption mode from 200 nm to 1100 nm. For the monitoring of the etching processes, the SPR chips were cut into fragments of the required size and placed close to the inner surface of the cuvette on the side of the spectrophotometer photodetector (to reduce possible light scattering). The spectra were recorded with respect to the cuvette with the same solution within an interval of 1-10 minutes. A total of up to 100 scans were collected for each measurement at a resolution of 2 cm^{-1} using polystyrene (Cuvette PS, VWR, Germany) or quartz (Quartz Glass High Performance Precision Cells, 104.002-QS, Hellma Materials GmbH, Germany) 10 mm cuvettes. When recording differential spectra, a part of the same chip with gold in pure water without addition of active components was placed in the reference channel. Additional experiments have shown that the contribution of the absorption of acid and hydrogen peroxide in the visible region of the spectrum is negligible.

The etching rate was estimated using a linear approximation of the optical data and assuming that the optical properties of the coating material remain constant. The region around the adsorption minimum at 505 nm was selected as it offers the best agreement with the Beer-Lambert-Bouguer law. This is due to minimization of the reflection and interference in thin films in the regions of minimal absorption. The etching rates ς_{VIS} (nm/min) was obtained from the optical density change taking into account the optical density of the initial film of known thickness (50 nm).

2.6.4 Electrochemical measurements

Gold films voltammograms were recorded using a conventional three-electrode setup. A specially designed Pyrex-glass cell with contacts for large area film samples was used for the electrochemical measurements. Au polycrystalline films (commercial SPR chips, typically 10×20 mm) were used as working electrodes. A platinum wire of 0.25 mm in diameter was used as the counter electrode, and an Ag/AgCl (a saturated KCl) electrode with a double salt bridge (Metrohm) was used as the reference electrode. All electrochemical measurements were performed using PC-controlled Autolab PGstat12 equipped with a FRA32 impedance module and controlled by NOVA 2.1.2 software (Metrohm, www.metrohm.com) at room temperature with additional deaeration (bubbling by N_2 during 3 min) of 0.05M of H_2SO_4 in water.

It should be noted that in this paper, roughened polycrystalline gold nano-structured films were used as the working electrode; these films have some specific measurement conditions regarding the electrolytes composition. Some of the typical features of these electrodes are described elsewhere [46, 64].

2.6.5 Surface plasmon resonance measurement

An SPR spectrometer ‘‘Biosupplar-521’’ (www.biosuplar.de) with angular scanning and a GaAs laser as the source of excitation (at a wavelength of 650 nm) [65, 66] was used. The SPR chips were fixed to a supporting glass prism (refractive index 1.61). Optical contact was ensured with an immersion liquid (n_D=1.6100 Refractive Index Liquid, hydrogenated terphenyl 1-bromo-naphthalene from Cargille Laboratories, USA).

The measurements were performed in the flow mode with peristaltic pump (Watson Marlow SCI Q400) connected after the measuring cell. The cell was formed by silicone rubber of ~1 mm thick covered with a Poly(methyl methacrylate) holder mounted directly on the sensor chip surface. For measurements, a complete scan (*ca.* 15°) mode with SPR curve registration and after a corresponding angle calibration procedure was used. Both the dependence of SPR minimum on time and the corresponding SPR curves have been registered for subsequent analysis.

The SPR chips were cleaned in Piranha solution (as described above) immediately before measurements and kept in distilled water at room temperature until the mounting in the instrument. After a stable baseline value was established, etching and modification procedures were carried out. The cell was perfused by PBS, then by solution of HSA (16-1000 μg/ml in PBS) and finally by the solution of anti-HSA (50 μl of the stock solution dissolved in 2ml PBS, 30 min). After achieving equilibrium, it was washed with PBS. After washing with the buffer, a solution of 3M NaCl in water was put into the cell, the value of the response to which served as the reference mark when comparing experiments performed on different SPR chips. After binding anti-HAS was removed by perfusion of aqueous solution containing 3M NaCl, 10mM Glycine pH 2.0 for 5 min. Then the cell was washed with PBS again.

2.7 Data processing

For recording and processing of the contact angle measurements, KSV instrument CAM 101 (www.biolinscientific.com) with KSV CAM 200 software was used, for the -processing of AFM images - Gwyddion (Department of Nanometrology, Czech Metrology Institute), UV-VIS - InSight software (Thermo Scientific, Germany), electrochemistry - NOVA 2.1.2 software (Metrohm, www.metrohm.com) (Metrohm Autolab B. V. Utrecht, The Netherlands), SPR spectroscopy – Biosuplar-510 (www.biosuplar.de).

SPR kinetics Γ(t) were analyzed with a model that takes heterogeneous processes on the surface into account using a stretched exponential function [67-69]:

$$\Gamma(t) = N \cdot \left(1 - \exp\left(-\left(\frac{t}{\tau}\right)^{\beta}\right)\right) \quad (1)$$

where N is the response range, τ is the time scale coefficient, and β is the parameter that indicates the mechanism of the surface layer evolution. The procedures of OriginPro 7.5 (OriginLab Corporation) were used for the fitting. The SPR spectra (dependence of reflection intensity on the angle) were analyzed using Winspall 3.02 software developed in the group of Prof. W. Knoll (Max-Planck Institute of Polymer Research, Mainz, Germany).

3. Results and Discussion

3.1 A proposed generalized process for cleaning-polishing of polycrystalline gold films

We developed a procedure inspired by the RCA cleaning used to prepare silicon wafers for bonding [58] while preserving the adhesion layer of the gold. The main idea is to reduce the concentration of the active components as well as the solution's temperature so as to focus the etching process on the nanoscale structure of the surface. This effectively creates a transition from active ubiquitous heterogeneous dissolution of metal to site-specific polishing of individual fragments of the surface structure [9, 10, 16, 25, 59, 60]. Specifically, we propose a cleaning-polishing procedure composed of the three following steps, taken consecutively:

1. Elimination of weakly bound mechanical particles and organic components under a stream of solvents, by using consecutively acetone, ethanol, isopropanol (leaves no residue), and finally ultrapure water;
2. Destruction of organic components on the gold surface through their oxidation into simple products using a suitable Piranha solution (see Methods for details);
3. Removal of inorganic contaminants and oxidation products, as well as surface polishing using a low concentrated water solution of hydrochloric acid and hydrogen peroxide (see Methods for details).

Applying this procedure consistently and reproducibly provides nano-smooth surfaces suitable for functionalization and SPR measurements, as shown hereafter.

3.2 Wetting properties of cleaned and etched gold surfaces

The wettability of the films can be used as a measure of the unbalance in molecular forces at the interface. Here this was quantified with comparative measurements of the contact angle θ_{H2O} formed by a sessile drop of water on the gold surfaces. The contact angle is generally expected to be hydrophilic ($\theta_{H2O} < 90^o$) [70], but the hydrophilicity/hydrophobicity of gold surfaces remains a highly debated topic with significant controversy [70-80]. Even when reported as hydrophilic [70] the value of θ_{H2O} typically ranges from 30^o to 80^o, far from the total wetting ($\theta_{H2O} \sim 0^o$) claimed by Bewig and Zisman [71]. This discrepancy may be caused by several reasons:

1) A presence of impurities, usually of organic nature [72, 73], rendering the surface more hydrophobic. A monolayer of carbonaceous contaminations can increase the contact angle up to $\theta_{H2O} \sim 50°$ [70].

2) Surface topography features in the range of 1-10 nm [74, 75] that can cause pinning of the contact line by defects due to roughness and trapping of air bubbles. A study reported example an apparent change of the properties of a gold surface from hydrophilic to the hydrophobic ($\theta_{H2O} > 90°$) purely through changes in surface topography (nanostructure of the macroporous gold films) [76]. The underlying scientific principle, underpinning the development of superhydrophobic surfaces [77], are captured by the theories of Wenzel [78] and Cassie and Baxter [79].

3) Macroscopic irregularities of the surface, surface charge, atmospheric pressure and surface chemistry.

These three effects are of particular importance for polycrystalline gold films possessing heterogeneous crystallinities [80, 81].

We measured the advancing contact angle of a water drop on the top of a freshly cleaned gold substrate. Fig. S1 (Supplementary materials) shows an initial contact angle of $\theta_{H2O} = 54\pm3°$,

significantly less than for the unmodified gold film θ_{H2O} = 80±3° and after Piranha treatment alone θ_{H2O} = 60±3°. This demonstrates that the surface becomes more hydrophilic after the Piranha treatment, with further improvement after the treatment by HAHP.
Over time the drop spreads slightly, and the contact angle decreases. For both samples after etching the kinetics are similar while the kinetics for the untreated surface show nonlinear dynamics - a rapid initial decline followed by a slow decrease (Fig. S1 in Supplementary materials). Analysis of the droplet shape for all samples shows that the initial decline (during the first 40 s) occurs at the constant volume, whereas the second phase (starting from the ~1 min) is related to water evaporation.
Overall, the contact angle measurements indicate that the Piranha treatment removes hydrophobic contaminants from the surface, followed by a smoothing of the surface roughness with HAHP. To confirm this interpretation, we investigated the evolution of the surface profile from nanometers to micrometers during the course of the treatment.

3.3 The topography of untreated, cleaned and etched gold coated plates
The gold-coated plates immersed in water were imaged by AFM. Representative topographic images (Fig.1) reveal a highly developed surface far from atomically smooth. The grain diameter of single gold crystallites ranges from few- up to tens of nanometers. After storage, contaminants are present on the surface, inducing characteristic scanning streaks due to the tip picking up weakly adsorbed molecules (Fig. S2, Supplementary Materials). The phase information of the AFM image for the untreated gold shows limited contrast, suggesting a uniform layer of contamination. After Piranha treatment more structure is visible but occasional streaks suggest that fragments of the oxidation products from the initial organic pollutants have not been removed by washing. This typical of the treatment of highly contaminated surfaces with oxidizing agents: the reaction products cannot be removed by simple washing. After etching in HAHP, the image of the gold surface becomes more typical of freshly made gold films imaged immediately after thermal evaporation in vacuum [9-11, 18, 31, 59, 82-84]. The height variations over a 1 μm line scan is 3-5 nm for the clean surface, with a root-mean-square (RMS) roughness of 1-3 nm.
The effect of the treatment on the surface topography can be quantified by plotting the height distribution profile over a given surface area either before treatment, after Piranha treatment and after the HAHP treatment (Fig.1). The untreated gold exhibits a flattened distribution (blue in Fig. 1) reflecting the impact of adsorbed impurities. After processing in Piranha, (Fig. 1, green Lorentzian-shaped) the distribution becomes more symmetrical and narrower due to the removal of most surface impurities. Further treatment with HAHP yield a significantly sharper Gaussian-shaped distribution without heavy tails (red in Fig. 1), reflecting an improved surface homogeneity. This result can be easily understood in the framework of the Central limit theorems governing the mathematical statistics of such distributions [67-69]: after processing in Piranha, the Cauchy distribution (Lorentzian curve) implies that the surface profile contains peaks and valleys of any size leading to the so-called heavy tails of distribution. After processing in HAHP, the resulting Gaussian distribution of the height indicates that the elements of surface roughness have all approximately the same size range. In other words, the surface has become homogeneous and isotropic on the spatial scale under consideration. Since the main obstacles to the formation of organized surface structures are cavities of high curvature [9,10], such a smooth surface is well suited for the chemical modification.

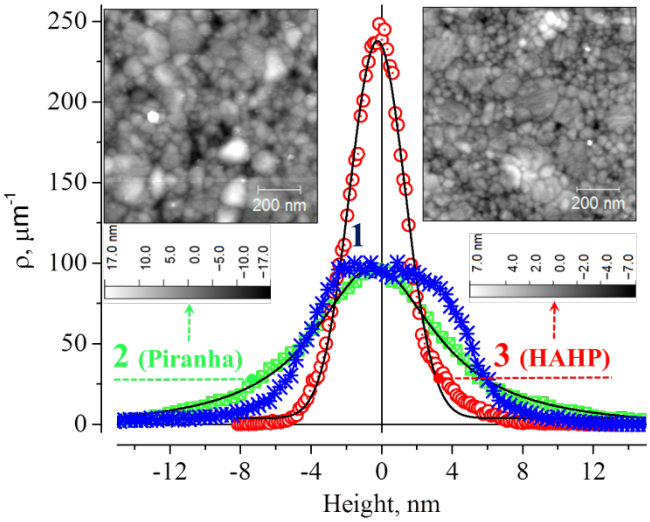

Figure 1. Height distribution profiles for the untreated gold surface (1, blue curve), the surface after Piranha treatment (2, green curve with Lorentzian fit and left AFM image) and after subsequent treatment by HAHP (3, red curve with Gaussian fit and right AFM image). In all case, the statistics was taken over a 1 μm × 1 μm image (Insert). ρ represent the height distribution density.

To analyze more in detail the relevant spatial scale associated with the largest topology changes, we calculated for each set of data the RMS roughness S_q as a function of the size L of the AFM image (Fig. 2). This approach is justified by the fact that each image has the same number of pixels regardless of size, thereby capturing size-dependent features. The results demonstrate that etching does not only improve small-scale roughness, but also the texture of the films, at least partially. However, after only Piranha processing, fragments from materials other than gold are present on the surface (see Fig. S2). This indicates that two processes are at play: the actual etching of the most heterogeneous fragments of the gold film (that is, with the maximum curvature of the surface) and the removal of the oxidation products of organic impurities by Piranha. Both of these processes improve the surface topography for the immobilization of SAMs or biological molecules.

It is known that low-scale (single crystallite specific) surface irregularities prevent formation of SAMs and can destroy adsorbed biomolecules [9-12]. Fig. 3 shows representative AFM images of individual crystallites together with their associated profiles. Comparison of the profiles taken after Piranha (top) and HAHP (bottom) treatment show a decrease in height variations both in magnitude and spatial frequency with etching. This further supports the idea of etching inducing a more uniform height distribution, determined primarily by surface texture rather than small-scale roughness on individual crystallites.

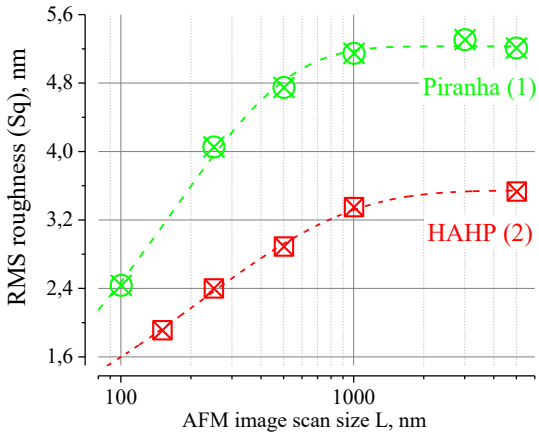

Figure 2. Dependence of RMS on the scan size for gold surface profile after the treatment in Piranha (green, 1) and subsequent HAHP (red, 2). The dashed lines serve as eye guides.

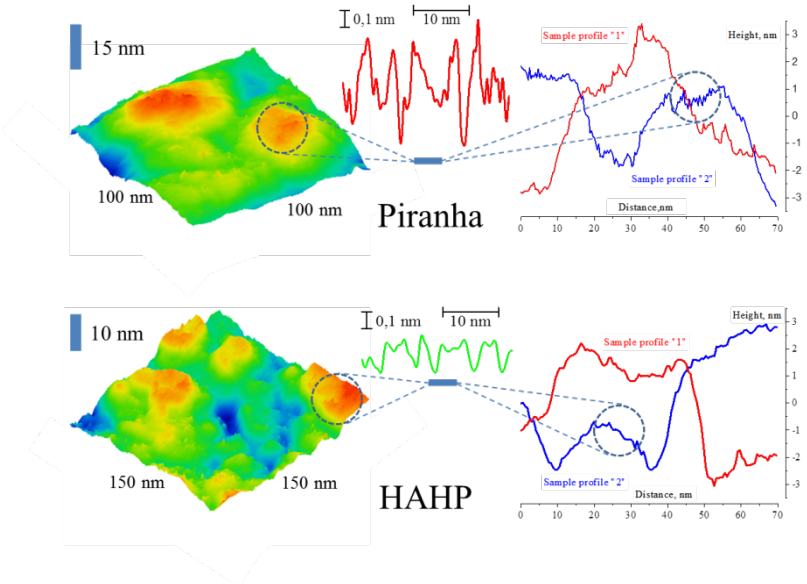

Figure 3. Representative AFM images of the surface of individual gold crystallites after Piranha etch (40 s, top) and 3% HAHP etch (20 min, bottom). The sample profiles represent some typical sections. Roughness profile in the middle (small-scale roughness typically on the crystallites surface) extracted from the experimental surface texture by subtraction the waviness.

3.4 Etching process kinetics: electrochemistry

Complementary information can be derived on the effect of etching on the gold surface using cyclic voltammetry (CV) electrochemical measurements [85]. CV measurements quantify the electrochemical accessibility of the surface and provide indications about the prominent crystallographic orientation of gold crystals on the electrode surface [86]. To exclude artefacts related to the surface cleaning process [87] only new gold samples freshly rinsing with the solvents and etched in Piranha were used, recording three cycles in total (Fig. S3, Supplementary Materials). Data from the first cycle was used to evaluate the surface properties. Voltammograms were taken for different parts after of a same gold chip after etched respectively for 3, 14 and 24 minutes in 3% HAHP (Fig. 4).

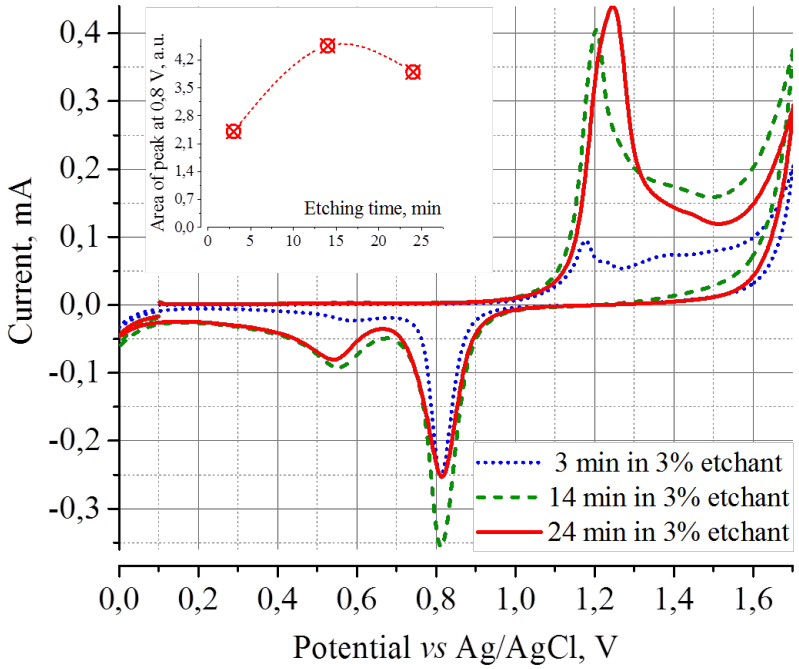

Figure 4. Representative cyclic voltammogram (0.0 to 1.7 V, 50 mV/s) recorded for a polycrystalline gold electrode in 0.05 M H_2S0_4 at 25°C in a conventional three-electrode cell setup, for different etching times in 3% HAHP etchant solution in water

The CV after treatment in Piranha (Fig. S3, Supplementary Materials) does not differ significantly after additional 3 min etching in 3% HAHP: a peak of oxidative current at 1.18 V with a shoulder at 1.23 V and two peaks of reductive currents at 0.81 V and 0.58 V are observed. After 14 min etching, dramatical changes occur to the CV curves with a growth in the electrochemical response. Despite the fact that the technology used for the gold deposition leads to polycrystalline layers, a comparison of the oxidative part of the CV curve (Fig. 4) with the literature [88] indicates the main contribution to originate from the (100) surface. The two oxidation peaks at 1.18 V and 1.23 V reported for Au (100) overlap, forming one sharp peak at 1.2 V. This is typical for the high concentrations of sulfuric acid where strongly chemisorbed HSO_4^- and/or SO_4^{2-} anions block nearly completely the otherwise distinguishable passage of the first electron [88]. The reductive part of the CV is also characterized by a strong increase of the peak at 0.81 V. A comparison of this reduction charge with total number of gold atoms on the surface indicates that over 50% of the surface gold atoms are involved into this process. The reductive charge is much smaller than the oxidative one which can be attributed to partial gold dissolution [89-93]. This effect can be also used for gold treatment for chemical sensing, but here the electrochemical techniques were applied only for investigation purposes.
Further chemical etching leads to the formation of a wider oxidative peak and to a decrease of the first reduction peak. Electrochemical processes on gold electrodes in sulfuric acid [94-96] include a multistep formation of gold oxide (anodic peak(s) and its subsequent reduction (the first reductive peak). The second reductive peak is attributed to the adsorption of solvated hydrogen ion [97].
The pronounced increase in electrochemical activity may indicate that after Piranha treatment, the gold still has some poor conducting material on its surface. This film is removed after 14 min etching in 3% HAHP. Further etching leads to some decrease in number of gold atoms which can be oxidized or reduced during potential cycling, consistent with a decrease of the electrode area during the etching process. The etchers are likely to attack mainly highly

energetic edge atoms of the cubic crystals thus leading to the transformation of (100) surface to the (111) surface possessing lower surface energy. This suggestion is confirmed by a cathodic shift of the oxidation peak consistent with previous studies on monocrystalline (100) and (111) gold electrodes [88].
During these modifications in HAHP, a Au(Cl)x surface coatings forms to replace the complexes formed on the surface during the Piranha treatment and displace the oxidation residues of organic pollutants. This passivation of the gold surface favorably affects its use for analytical applications in bio-sensing, since most measurements are made in media containing chloride anions playing a significant role in the processes occurring in the immediate vicinity of the gold surface [46].

3.5 Etching process kinetics: optics

A typical adsorption spectrum of the gold films is shown in Fig. 5a. Spectrophotometric investigations indicate that complete etching of gold film together with the chromium adhesion layer in 3% HAHP etchant solution takes several days. The positions of the absorption bands (modeled by the Gaussian peaks) after completion of the etching process indicate the formation of $HAuCl_4$ as the final etching product (Fig. 5a) [98].
The differential absorption spectra of gold film show that at the beginning of the etching the optical density monotonically decreases preferably in the long-wave region (Fig. 5b). This effect may be caused by a smoothing of small-scale inhomogeneity on the crystallites surface resulting in a decrease of the light scattering by surface relief. A similar hypothesis was used in [25] to explain an effect of surface smoothing on the intensity of the light scattering under surface plasmon resonance conditions. After ~30 min of additional process (probably, texture etching in the inter-crystalline regions) the differential spectrum takes a shape typical for gold nano-structures with an absorption peak of a local surface plasmon resonance excitations above 510 nm. Such nanostructuring of a continuous polycrystalline gold films has been described earlier [55]. Nanostructures can induce additional scattering of propagating plasmon-polariton excitations, including a radioactive emission [59] which lead to a broadening of the SPR resonance curve and a decrease in the efficiency of the SPR transducer. It is the main reason for limiting the etching time to 30-40 minutes in 3% HCl, 3% H_2O_2, 94% H_2O v/v/v at room temperature.

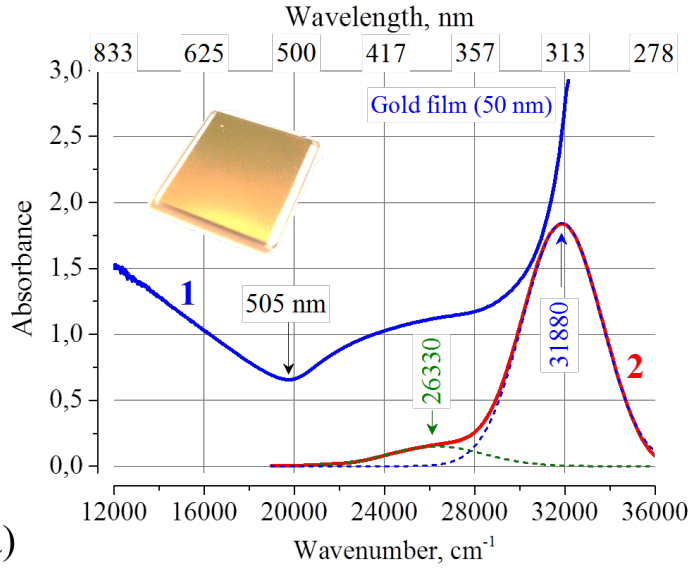

a)

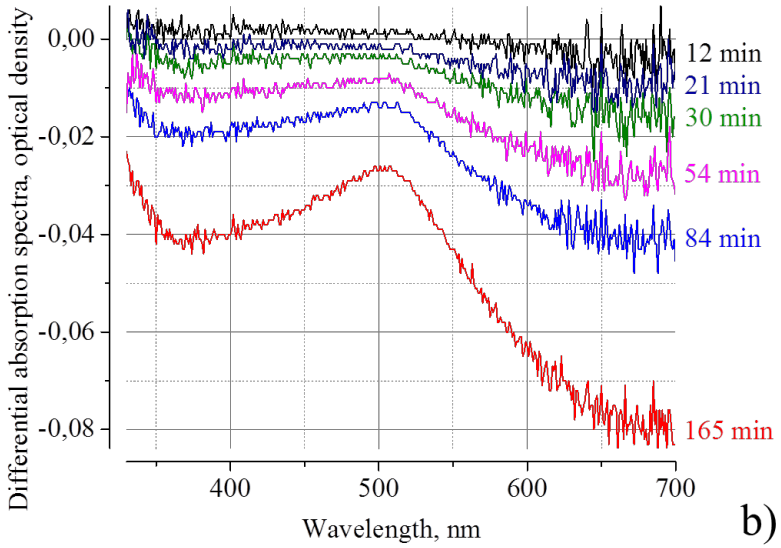

Figure 5. Representative absorption spectra (a) of a thin gold film (50 nm) with chromium adhesion layer (5 nm) on glass surface (1) and after the etching (2). Differential adsorption spectra of the etching solution (b) were obtained by subtraction of the initial spectrum from the subsequent spectra for different time of etching. The etchant composition is 3% HCl, 3% H_2O_2, 94% H_2O v/v/v %.

The kinetics of changes in optical absorption of the gold film at 505 nm (minimum adsorption value) during the etching is shown in Fig. 6. The data presented indicate that the thickness of the film decreases linearly with time. Assuming that the absorption coefficient is constant and neglecting a possible contribution of scattering, we get from the Beer-Lambert-Bouguer law that the dissolution of the gold film in the etchant with x = 3 (i.e. 3% HCl, 3% H_2O_2, 94% H_2O v/v/v) at room temperature proceeds with a constant rate of ~10 pm/min (inset in Fig. 5). It should be noted that the etching processes with a different etchant composition (increase of HCl and H_2O_2 content from 1 to 5%) showed similar etching rates. One possible explanation is that the etching is a diffusion-controlled process.

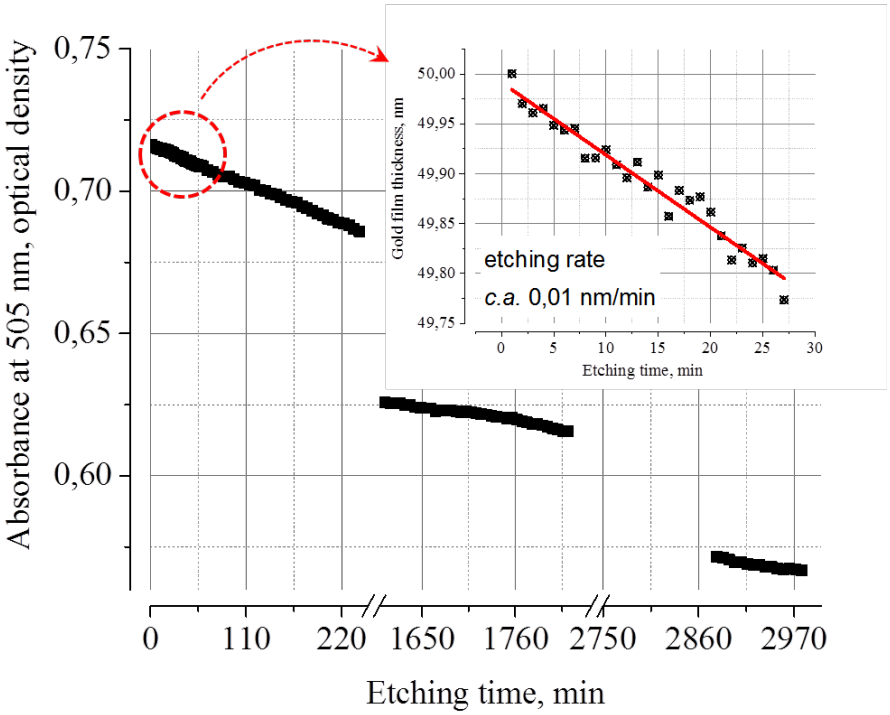

Figure 6. Kinetics of changes of optical density at 505 nm for a 50 nm thick polycrystalline gold film during treatment in HCl:H_2O_2:H_2O etchant with the ratio 3:3:94 v/v/v % in stationary conditions (without liquid flow of etchant).

3.6 Etching process kinetics: SPR measurements

Spectrometers based on the surface plasmon-polariton resonance in thin gold films are highly sensitive to minute changes in the films, especially on the outer surface where the maximal amplification of the electromagnetic field is observed [18-21]. In the continuum flow of the HAHP solution over the film, the change of SPR shift per time unit (ζ), which can be associated with etching rate, remains constant up to the concentration of active components x ~3, and undergoes a jump (probably due to the formation of gas bubbles on the metal surface) with a subsequent exponential decreasing (probably due to detachment of bigger gas bubbles) when the concentration is further increased up to 7% (Fig. S4, Supplementary materials). The observed etching rate ζ has a logarithmic dependence on the flow rate in the range of 2-64% of the maximum flow rate (2.5 ml/min) (Fig. S5, Supplementary materials): when the flow rate increases by 16 times, the etching rate increases only 1.7 times. With an increase of component concentration to more than 7%, intensive bubbling disturbs the correct measurements and, probably, induces non-uniform etching. In accordance with the results of optimization study, all follow-up measurements were carried out at a flow rate of about 125µl/min and a concentration of the etchant active components of 3%.

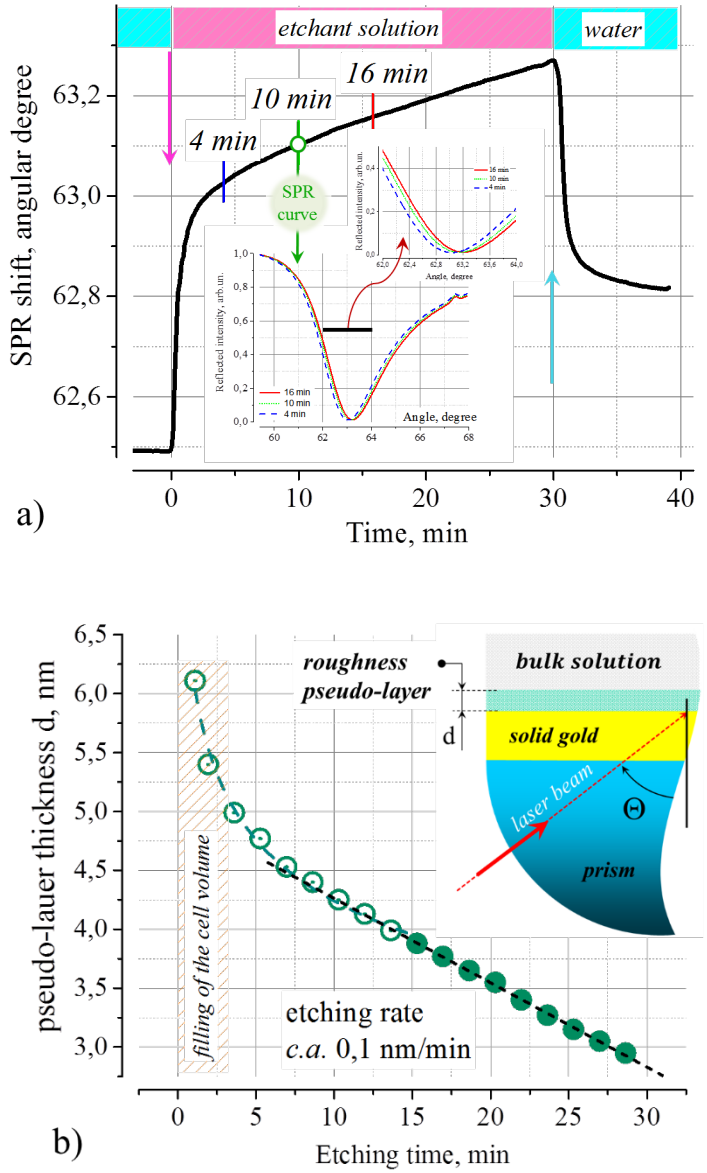

Figure 7. Kinetics of SPR angle during etching by 3:3:94 % v/v/v solution of HCl:H_2O_2:H_2O (a). The kinetics was recalculated into dependence of the thickness changes of the roughness gold pseudo-layer (b). The thickness at each point was calculated by fitting of angular SPR spectra ((a), inset) using Winspall 3.02 software package for the optical model consisting of a thick glass layer (refractive index: 1.61+0i), a solid gold film 50.74 nm thick (0.1936+3.5499i), rough pseudo-layer with thickness d (1.225+0i) and an etchant solution (1.336+0i).

The case we are considering differs fundamentally from the typical measurements of SPR spectroscopy: during etching, the changes affect the gold film itself, the carrier of plasmon-polariton excitations. In this case, the most correct way to extract the parameters of interfacial layer is by fitting individual angular SPR spectra (the dependence of the reflected light intensity on the angle of incidence of laser radiation, Fig. 7a, inset) using the Fresnel equations for the optical model of the system corresponding to different etching steps (Fig.7b, inset).
Approximations of a series of curves in the baseline region (in water, before the introduction of the etchant and after the etching) made it possible to establish that the angular SPR spectra is

well described by a two-layers optical model of gold film that taking into account the roughness on the metal surface (see insert in Fig. 7b), as proposed, for example, in [99, 100]. It should be noted that the angular SPR spectra were well approximated in a wide range of angles, with parameters being close for similar gold films [11, 16, 31]; it means that effective parameters of the solid part of the gold film take into account ignored by Fresnel equations scattering and features of instrument function.

The main problem in using the approach based on the approximation of the angular SPR spectra is associated with the ambiguity in the separate determination of parameters n and d for the rough pseudo-layer since these values appear in Fresnel equations as the product [101]. Taking into account typical errors accompanying SPR analysis [20], the result can be used (i) to estimate the parameters of individual plane-parallel layers within the multilayer model from an independent technique and (ii) to ensure that the calculated values of n and d correspond to the global residual function minima.

The thickness of the rough pseudo-layer d can be estimated from the distribution of the surface profile obtained by AFM imaging (Fig. 1) as ~ 6 nm for the surfaces after processing with Piranha. To estimate the refractive index of the rough pseudo-layer, the most common Maxwell-Gardner model of the effective medium (applicable to a small quantity of spherical objects in an isotropic medium) and its generalization for non-spherical inclusions - the Brusseman model - were used [102, 103]. The calculation within the framework of these models using the refractive index 0.2+3.6i for 'solid' gold and 1.336 for the surrounding medium showed that when the roughness area fill factor is less than 40% (100% corresponds to the bulk gold) then the refractive index of the pseudo-layer is greater than 1.0. Taking into account relatively low gold fill factor, discontinuous structure of the profile within the films' roughness as well the fact that Fresnel equations do not take into account scattering [5, 20, 21, 104, 105], the absorption coefficient of the rough pseudo-layer was assumed to be zero. Comparison of the results for full and simplified (the absorption coefficient of the roughness layer is zero) optical models showed that the angular SPR spectra changes observed at different etching times can be adequately described using only one parameter - the thickness of the roughness pseudo-layer with a refractive index (1.225+0i) and fixed values of other parameters, in particular those specific for "solid" i.e. continuous bulk gold film. This allows one to improve significantly the accuracy of the calculations. Therefore, the full optical model used for calculations includes a glass prism (1.61+0i) / a 'solid' gold film 50.74 nm thick (0.1936+3.5499i) / a rough pseudo-layer with thickness d (1.225+0i) / and an etchant solution (1.336+0i).

Fig. 7b shows the evolution of the pseudo-layer thickness d during the etching process. Data analysis allows highlighting two areas corresponding to different processes on the surface. The rapid changes in the roughness area observed in the initial part may be due dissolving of the small-scale roughness (narrow and long peaks, often formed after treatment in Piranha) and chemical cleaning/modification of the gold surface.

As the gold film in the etchant solution exposure time increases, the rough layer thickness monotonously decreases. After initial rapid drop over 15 minutes, a further decrease occurs rather slowly: the established etching rate is approximately 1 Å/min, which likely reflects the process of etching the entire film texture as a whole. Taking into account the estimated metal fraction within the rough pseudo-layer (c.a. 12% for n=1.225+0i) it's etching rate in 0.1 nm/min is exactly the same as 0.01 nm/min for gold material dissolution determined by optical measurements.

3.7 Proteins adsorption on the surface after HAHP treatment

Globular serum proteins Bovine Serum Albumin (BSA) or Humane Serum Albumin (HSA) are often used as model proteins to analyse interfacial processes near functional surfaces or as

blocking agents in sensing architectures to prevent non-specific sorption of other biomolecules [106-108]. In the present study HSA is used to estimate the bio-friendly features of polycrystalline gold films after cleaning and smoothing procedures.
To analyze possible protein unfolding on the gold surface we used the procedure and model described in detail in [12]. Fig. 8 shows a typical adsorption experiment sequence with the insert quantifying the dependence of the adsorbed protein amount on its concentration in the solution. As clear from the figure, the amount of irreversibly bound protein is proportional to the protein concentration in the HSA solution. In line with the two-stage model of surface-induced protein transitions in adsorbed biofilms [12] this clearly indicates that the tertiary structure breaks and the surface is covered by an amino acid sequence unfolded to the secondary or primary structure at low protein concentrations in the solution.

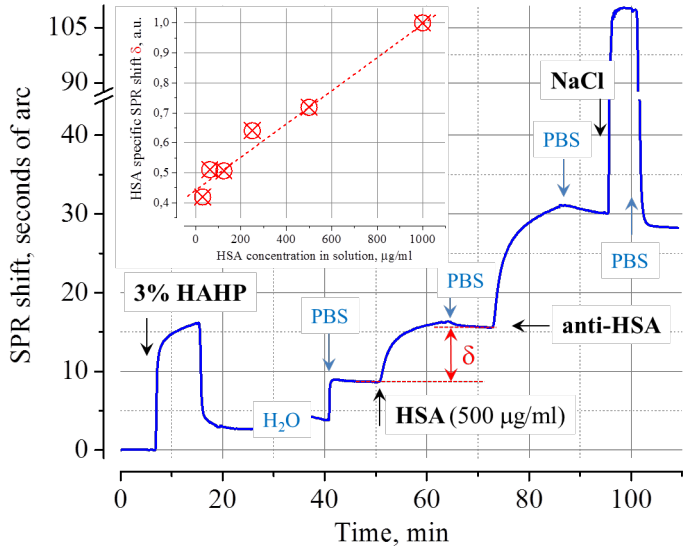

Figure 8. SPR sensing of HSA adsorption and its dependence. The amount of irreversibly adsorbed proteins is quantified as a function of the protein concentration in solution (insert).

The kinetic curves of HSA adsorption onto the gold surface after its etching in 3% HAHP (20 min) can be analyzed using stretched exponential function approximations (Fig. 9). As shown in [21, 43, 51-54, 109-111], this approach allows elucidation of the mechanism underpinning the dominant surface process within the framework of the most common nonequilibrium dynamics model to date [5, 67, 68]. The data were obtained for the kinetic curve sections starting from 3.5 minute after the beginning of the sample injection, when stable HSA concentration in the cell is achieved.

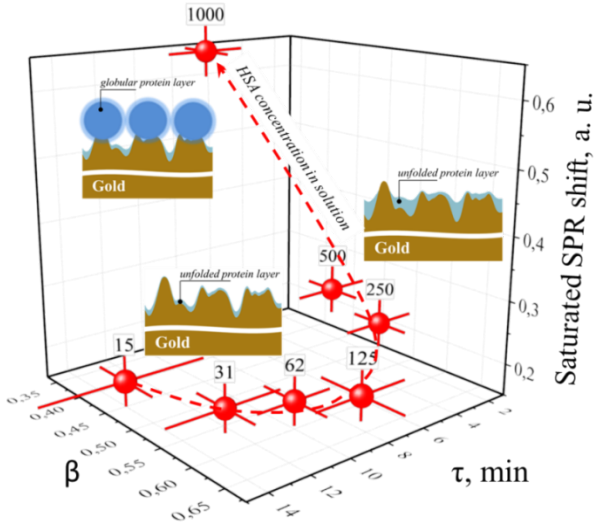

Figure 9. The dependence of the values of β, τ and the saturated values of the SPR angle shift on the HSA protein concentration in solution (labeled in the figure in μg/ml) obtained by fitting of the experimental adsorption kinetics by equation (1). The gold surface was etched by 3% HAHP for 20 min. The inset shows the adsorption model of the protein on the gold surface at its different concentrations in the solution.

The fitting data indicate that the kinetic parameters of the adsorption process depend on the protein concentration. At the concentrations below 100 μg/ml, a formation of the surface layer is limited by the diffusion and includes a binding of fully unfolded HSA molecules. This is confirmed by (1) a roughly constant surface coating thickness (SPR shift), (2) a decrease of the characteristic adsorption times when the analyte concentration in the solution increases and (3) values close to 0.5 for β (Fig.9) [5, 67]. Approximation of SPR curves suggests that the formation of the surface coating in this mode can be described by the same optical model as discussed above, but with an increased value of the rough layer refractive index (for example, from 1.225 to 1.248 at a concentration of 64 μg/ml). This suggests that due to the low concentration of protein in the solution, individual molecules have enough time to unfold the tertiary structure on the surface and the organic material actually "fills" the rough layer with its fragments.

When the protein concentration in the solution increases over 500 μg/ml, a sharp increase of the surface layer thickness is observed. To correctly describe the SPR curve, a separate protein layer must be added to the roughness layer (for example, at a concentration of 1000 μg/ml, the effective thickness of this plane-parallel continuous layer of HSA is about 3 nm with a refractive index of about 1.44. For a less dense packing typical of charged protein on the surface, the size of protein's inclusions is be higher, in good agreement with the known size HSA size (5-10 nm).

When the protein concentration in the solution increases, the competition between the protein adsorption in native form and the surface-induced unfolding process increases: the need to match these processes leads to an increase of the characteristic time scale τ, while an expansion of the processes involved in the formation of the final coating leads to a decrease of β. The area of intermediate concentrations (Fig.9), from ~100 to ~400 μg/ml, corresponds to a range in which the diversity of various processes is largest and is hence poorly controlled. Antibodies could not reversibly bind to HSA, suggesting denaturation of the HAS layer.

4. Concluding remarks

The present study demonstrates the efficiency of soft wet etching protocols based on $HCl:H_2O_2:H_2O$ composition for cleaning and smoothing the polycrystalline gold films utilizing for nanoscale specific functional modification. Overall, we find that when polycrystalline gold films are incubated in a solution of the HAHP etchant ($HCl:H_2O_2:H_2O$ 3:3:94 v/v/v) at room temperature (21±1 °C), the surface profile undergoes a series of changes that occur in the following sequence:

At the initial stage (less than 5 minutes), the remnants of oxidation products are removed from the gold surface, a substitution reaction at the reactive surface centers takes place. Then, within 5-15 minutes after beginning of incubation the process of dissolving of the most reactive (thin and long) fragments of gold or its compounds begins. At this stage, the total surface of metallic gold reaches its maximal value and is characterized by strong branching which then decreases with further treatment time.

Subsequent etching (15-30 min) leads to a greater smoothing of the surface, the predominance of more stable facets with a minimal contribution of small-scale spikes on the surface of individual round gold crystallites.

Past 30 minutes etching, inter-crystalline boundaries begins to appear simultaneously to change in texture, self-consistent with processes starting to take place on the surface of individual crystallites until the film is completely etched.

The proposed protocol may help better reproducibility and stimulate further application of noble films in (bio)sensors, particularly architectures combining nanostructured functional subunits spatially arranged in a specific manner [112-115]. The results also indicate that native polycrystalline gold films are not suitable for direct applications in biosensors, even after chemical polishing. A special buffer layer preventing destruction of bio-molecules is needed. Moreover, the widely used procedure of gold coating by BSA or HSA does not provide a complete surface passivation by native molecules and can lead to the presence of sharp gold fragments with a high denaturing ability. If globular proteins are used, their concentration in the solution should be as high as possible in order to minimize protein denaturation on the surface.

Conflicts of interest

There are no conflicts to declare.

Acknowledgment

B.S. thanks DAAD (Grant 57314021), Brandenburg Technical University Cottbus-Senftenberg and the Institute of Advance Study of the Durham University for scientific fellowships.

References

1. V.M. Mirsky and A. Yatsimirsky, Artificial Receptors for Chemical Sensors, Wiley-VCH, Weinheim, 2011.
2. F.-G. Banica, Chemical Sensors and Biosensors: Fundamentals and Applications, Wiley-VCH, Weinheim, 2012.
3. B.A. Snopok and I.V Kruglenko, Thin Solid Films, 2002, 418, 21-41.
4. J. Narang and C.S. Pundir, Biosensors: An Introductory Textbook, Jenny Stanford Publishing, 2017.

5. B. Snopok, Biosensing under Surface Plasmon Resonance Conditions, in: Sattler, K. (ed.), 21st Century Nanoscience – a Handbook, Taylor and Francis Group, 2020, ch. 19, pp.
6. G.V. Lisichkin, Khimiya privitykh poverkhnostnykh soedineniy, Fizmatlit, Moscow, 2003.
7. B.A. Snopok, P.N. Boltovets and F.J.Rowell, Theor Exp Chem, 2008, 44 (3), 165–171.
8. M.J.Schöning and A.Poghossian (eds.), Label-Free Biosensing. Advanced Materials, Devices and Applications, Springer International Publishing, 2018.
9. P.E.Strizhak, B.A.Snopok, T.Melnik, E.V.Kostyukevich, S.I.Lysenko, P.E.Shepeliavii, S.L.Priatkin, S.A.Kostuykevich, Yu.M.Shirshov and E.F.Venger, Multifractal properties of irregular surfaces: polycrystalline gold films, in: O.V. Angelsky (ed), International Conference on Correlation Optics, Proceedings of SPIE 3904, 1999, pp. 374-385.
10. B.A. Snopok, P.E. Strizhak, E.V. Kostyukevich, V. Serebriy, S.I. Lysenko, P.E. Shepeliavii, S.L. Priatkin, S.A. Kostuykevich, Yu.M. Shirshov and E.F. Venger, Semiconductor Physics, Quantum Electr. and Optoelectronics, 1999, 2 (3), 86-97.
11. B.A. Snopok, K.V. Kostyukevych, O.V. Rengevych, Yu.M. Shirshov, E.F. Venger, I.N. Kolesnikova and E.V. Lugovskoi, Semiconductor Physics, Quantum Electronics & Optoelectronics, 1998, 1 (1), 121-134.
12. B.A. Snopok and E.V. Kostukevich, Analytical Biochemistry, 2006, 348 (2), 222-231.
13. B.A. Snopok, P.N. Boltovets and F.J. Rowell, Theoretical and Experimental Chemistry, 2006, 42 (4), 210-216.
14. A. Hoffmann, Z. Lenkefi and Z. Szentirmay, Journal of Physics: Condensed Matter, 1998, 10 (24), 5503-5513.
15. Kolomenskii, J. Noel, S. Peng and H. Schuessler, Appl. Opt., 2009, 48, 5683-5691.
16. Ch.-Ch. Lee and Y.-J. Jen, Appl. Opt., 1999, 38, 6029-6033.
17. D.I. Yakubovsky, A.V. Arsenin, Y.V. Stebunov, D.Yu. Fedyanin and V.S. Volkov, Optics Express, 2017, 25 (21), 25574-25587.
18. B.A. Snopok, K.V. Kostyukevich, S.I. Lysenko, P.M. Lytvyn, O.S. Lytvyn, S.V. Mamykin, S.A. Zynyo, P.E. Shepelyavyj, E.F. Venger, S.A. Kostyukevich and Yu.M. Shirshov, Semiconductor Physics, Quantum Electronics and Optoelectronics, 2001, 4 (1), 56-69.
19. J. Homola (Ed.), Surface Plasmon Resonance Based Sensors Series: Springer Series on Chemical Sensors and Biosensors, Springer-Verlag, Berlin Heidelberg, 2006.
20. P.M. Boltovets and B.A. Snopok, Talanta, 2009, 80, 466-472.
21. B.A. Snopok, Theoret. and Experim. Chemistry, 2012, 48 (5), 265-284.
22. A. Singh, A.K. Choubey, M.H. Modi, B.N. Upadhyaya and G.S. Lodha, Journal of Physics: Conference Series, 2013, 425, 152020.
23. T. Sakata, Y. Okabe, K. Kuwabara, N. Sato, K. Ono, N. Shimoyama, K. Machida and H. Ishii, Japanese Journal of Applied Physics, 2009, 48 (2R), 026501.
24. A. Schaefer, D. Ragazzon, A. Wittstock, L.E. Walle, A. Borg, M. Bäumer and A. Sandell, The Journal of Physical Chemistry C, 2012, 116 (7), 4564-4571.
25. Savchenko, E. Kashuba, V. Kashuba and B. Snopok, Sensor Letters, 2008, 6, 705–713.
26. W. Kern, Journal of the Electrochemical Society, 1990, 137 (6), 1887–1892.
27. M. Itano, F.W. Kern, M. Miyashita and T. Ohmi, Particle removal from silicon wafer surface in wet cleaning process. In: IEEE Transactions on Semiconductor Manufacturing, 1993, 6 (3), 258.

28. R. Rudder, R. Thomas, and R. Nemanich, Remote Plasma Processing for Silicon Wafer Cleaning, in: W. Kern (ed.), Handbook of Semiconductor Wafer Cleaning Technology. Noyes Publications, 1993, ch.8, pp. 356–357.
29. K.K. Christenson, S.M. Smith and D. Werho, Microcontamination, 1994, 12 (6), 47-53.
30. S. Moniruzzaman, G. Caleb and H. Cameron, S. Muhtadyuzzaman, Sputtering Journal of Materials Science and Engineering B, 2018, 8 (3-4), 66-76.
31. B.A. Snopok, K.V. Kostyukevych, G.V. Beketov, S.A. Zinio, Yu.M. Shirshov and E.F. Venger, Semiconductor Physics, Quantum Electronics and Optoelectronics, 2000, 3 (1), 59-68.
32. T.A. Green, Gold Bull, 2014, 47, 205-216.
33. M. Yamamoto, T. Matsumae, Y. Kurashima, H. Takagi, T. Suga, T. Itoh and E. Higurashi, Micromachines (Basel), 2019, 10 (2), 119.
34. L.M. Fischer, M. Tenje, A.R. Heiskanen, N. Masuda, J. Castillo, A. Bentien, J. Emneus, M.H. Jakobsen and A. Boisen, Microelectronic Engineering, 2009, 86 (4-6), 1282–1285.
35. P.M. Martin (Ed.), Surface Preparation for Film and Coating Deposition Processes, in: Handbook of Deposition Technologies for Films and Coatings (third ed.), William Andrew Publishing, 2010, Ch., pp. 93-134.
36. K.C. Swanson, D.P. Riemer and S.A. Fank, Gold electroplating solution and method. Patent US10570525B2, 2016.
37. S.S. Ermakov, A.V. Borzhitskaya and L.N. Moskvin, Journal of Analytical Chemistry, 2001, 56 (6), pp. 542–545.
38. F.L. Almeida and S.G. Santos-Filho, Surface Activation of Gold electrodes Using Electrochemical Conditioning, in: 28th Symposium on Microelectronics Technology and Devices (SBMicro 2013), Proceedings IEEE, 2013, 1-5.
39. J.C. Hoogvliet, M. Dijksma, B. Kamp and W.P. van Bennekom, Anal. Chem., 2000, 72(9), 2016–2021.
40. M. Todeschini, A. B. da Silva Fanta, F. Jensen, J. B. Wagner, A. Han, ACS Appl. Mater. Interfaces, 2017, 9, 42, 37374–37385
41. W.M. Abbott, C. P. Murray, S. Ní Lochlainn, F.Bello, C.Zhong, C.Smith, E. K. McCarthy, C.Downing, D. Daly, A. K. Petford-Long, C. McGuinness, I. I. Chunin, J.F. Donegan, and D. McCloskey, ACS Appl. Mater. Interfaces 2020, 12, 11, 13503–13509
42. R. Bock, A Handbook of Decomposition Methods in Analytical Chemistry, Marr, I.L. (1st ed.). John Wiley and Sons, New York, 1979.
43. J. Kang and P.A. Rowntree, Langmuir, 2007, 23 (2), 509-516.
44. B.A. Snopok, M. Yurchenko, L. Szekely, G. Klein and E. Kasuba, Anal. Bioanal. Chem., 2006, 386, 2063–2073.
45. A. Saranga, Nanofabrication: Principles to Laboratory Practice, CRC Press, 2016.
46. V.K. Laurinavichyute, S. Nizamov and V.M. Mirsky, Chem Phys Chem, 2017, 18, 1552.
47. A. Mike (ed.), Gold Ore Processing, Volume 15, 2nd ed. Project Development and Operations, Elsevier Science, 2016.
48. S. Cherevko, A.A. Topalov, A.R. Zeradjanin, I. Katsounaros and K.J.J. Mayrhofer, RSC Adv., 2013, 3, 16516–16527.
49. P.W. Mertens, R. Vos, W. Masayuki, S. Arnauts, H. Takahashi, D. Tsvetanova, D. Cuypers, S. Sioncke, N. Valckx, S. Brems, M. Hauptmann and M. Heyns, ECS Trans, 2011, 41 (5), 3-13.

50. L.F. Kozin and V.T Melekhin, Russian Journal of Applied Chemistry, 2004, 77 (10), 1573-1592.
51. P.M. Boltovets, O.M. Polischuk, O.G. Kovalenko and B.A. Snopok, The Analyst, 2013, 138, 480-486.
52. B.A. Snopok, S. Darekar and E.V. Kashuba, The Analyst, 2012, 137, 3767.
53. P. Boltovets, S. Shinkaruk, L. Vellutini and B. Snopok, Biosensors and Bioelectronics, 2017, 90, 91–95.
54. M. Manilo, P.M. Boltovets, B.A. Snopok, S. Barany and N.I. Lebovka, Colloids and Surfaces A Physicochemical and Engineering Aspects, 2017, 520, 883-891.
55. P.M. Boltovets, S.A. Kravchenko and B.A. Snopok, Plasmonics, 2010, 5 (4), 395-403.
56. W. Kern and D.A. Puotinen, RCA Rev., 1970, 31, 187-206.
57. J.L. Vossen and W. Kern, Thin Film Processes II, Academic Press, 2012, pp. 888.
58. Kern, W. (ed.), 1993. Handbook of Semiconductor Wafer Cleaning Technology: Science, Technology, and Applications. Noyes Publications, Westwood.
59. S.I. Lysenko, B.A. Snopok and V.A. Sterligov, Optics and spectroscopy, 2010, 188 (4), 618-628.
60. J. Leib, R. Mönig and C.V. Thompson, Phys. Rev. Lett., 2009, 102, 256101.
61. H.-J. Butt and M. Jaschke, Nanotechnology, 1995, 6, 1.
62. K. Voïtchovsky, J.J. Kuna, S.A. Contera, E. Tosatti and F. Stellacci, Nature Nanotechnology, 2010, 5(6), 401–405.
63. D. Nečas and P. Klapetek, Cent. Eur. J. Phys., 2012, 10(1), 181-188.
64. M. Libansky, J. Zimaa, J. Barek, A. Reznickova, V. Svorcik and H. Dejmkova, Electrochimica Acta, 2017, 251, 452–460.
65. R.B.M. Schasfoort (Ed.), Handbook of Surface Plasmon Resonance, 2nd ed., The Royal Society of Chemistry, 2017.
66. V.-D. Tuan, Nanotechnology in Biology and Medicine: Methods, Devices, and Applications, second ed., CRC Press, 2017.
67. B.A. Snopok, Theoretical and Experimental Chemistry, 2014, 50 (2), 67-95.
68. B.A. Snopok and O.B. Snopok, Information Processing in Chemical Sensing: Unified Evolution Coding by Stretched Exponential, in: Nanostructured Materials for the Detection of CBRN, Springer, 2018, pp. 233-244.
69. R. Schweiss, V.M. Mirsky and O.S. Wolfbeis, Capacitive study of self-assembled alkylthiol monolayers: surface charge effects and kinetics of surfactants adsorption, Materials Science Forum, 1998, pp. 287-288, 427-430.
70. T. Smith, Journal of Colloid and Interface Science, 1980, 75 (1), 51-55.
71. K.W. Bewig and W.A. Zisman, The Journal of Physical Chemistry, 1966, 69 (13), 4238-4242.
72. G.I. Loeb and M.E. Schrader (eds.), Modern Approaches to Wettability. Theory and Applications, Springer US, 1992.
73. E. Ricci and R. Novakovic, Gold Bull, 2001, 34, 41-49.
74. J.-L. Liu, X.-Q. Feng, G. Wang and S.-W. Yu, J. Phys.: Condens. Matter, 2007, 19, 356002.
75. S. Das, J.H. Snoeijer and D. Lohse, Phys. Rev. E, 2010, 82, 056310.
76. M.E. Abdelsalam, P.N. Bartlett, T. Kelf and J. Baumberg, Langmuir, 2005, 21, 1753-1757.
77. J. Drelich, E. Chibowski, D.D. Meng and K. Terpilowski, Soft Matter, 2011, 7 (21), 9804-9828.
78. R.N. Wenzel, Ind. Eng. Chem., 1936, 28, 988-994.
79. A.B.D. Cassie and S. Baxter, Trans. Faraday. Soc., 1944, 40, 546-551.
80. G. Valette, J.Electroanal. Chem., 1982, 139, 285-301.

81. R.F. Carvalhal, R.S. Freire and L.T. Kubotaa, Electroanalysis, 2005, 17 (14), 1251-1259.
82. Celedón, M. Flores, P. Häberle and J. E. Valdés, Brazilian Journal of Physics, 2006, 36(3b), 956-959.
83. S. Solhjoo and A.I. Vakis, Tribology International, 2017, 115, 165-178.
84. S. Negm, H. Talaat and J. Pelzl, Photoacoustic study of surface roughness on thin evaporated gold films. In: Proceedings IEEE Ultrasonics Symposium, Baltimore, MD, USA, 1993, vol.2, pp. 1259-1261.
85. L.R. de Astudillo, L. Rivera, R. Brito-Gómez and R.J. Tremont, Journal of Electroanalytical Chemistry, 2010, 640, 56–60.
86. L.D. Burke and P.F. Nugent, Gold Bulletin, 1997, 30(2), 43-53.
87. Srejić, M. Smiljanić, Z. Rakočević and S. Štrbac, Int. J. Electrochem. Sci., 2016, 11, 10436 – 10448.
88. S. Štrbac, R.R. Adzic and A. Hamelin, J. Electroanal. Chem., 1988, 249, 291-310.
89. R. Gaggiano, E. Martinez Lombardia, I. De Graeve, L. Lapeire, K. Verbeken, L.A.I. Kestens and H. Terryn, Electrochemistry Communications, 2012, 24, 97–99.
90. D.A.J. Rand and R. Woods, J. Electroanal. Chem., 1972, 35, 209–218.
91. Y.M. Kolotyrkin, Electrochim. Acta, 1973, 18, 593–606.
92. S.H. Cadle and S. Bruckenstein, Anal. Chem., 1974, 46, 16–20.
93. S. Vesztergom, M. Ujva´ri and G.G. La´ng, Electrochem. Commun., 2011, 13, 378–381.
94. H. Angerstein-Kozlowska, B.E. Conway, B. Bamett and J. Mozota, J. Electroanal. Chem., 1979, 100, 417-446.
95. H. Angerstein-Kozlowska, B.E. Conway, A. Hamelin and L. Stoicoviciu, Electrochim. Acta, 1986, 31, 1051-1061.
96. H. Angerstein-Kozlowska, B.E. Conway, A. Hamelin and L. Stoicoviciu, J. Electroanal. Chem., 1987, 228, 429-453.
97. A. Hamelin, J. Electroanal. Chem., 1996, 407, 1-11.
98. K. Paclawski and T. Sak, J.Min.Metall.Sect.B-Metall., 2015, 51 (2) B, 133-142.
99. M. Kanso, S. Cuenot and G. Louarn, J. Opt. A: Pure Appl. Opt., 2007, 9, 586–592.
100. Y. Zhitao, L. Changjian, G. Yachen, W. Jiyu, Y. Wenlong, Chinese Optics Letters Col, 2016, 14(4), 042401.
101. O.V. Rengevych, Yu.M. Shirshov, Yu.V. Ushenin and A.G. Beketov, Semiconductor Physics, Quantum Electronics & Optoelectronics, 1999, 2 (2), 28-35.
102. J.C. Maxwell-Garnett, Philos. Trans. R. Soc. A., 1904, 203, 385 –420.
103. D.A.G. Bruggemann, Ann. Phys., 1935, 416 (7), 636 – 679.
104. A. Savchenko, E. Kashuba, V. Kashuba and B. Snopok, Analytical Chemistry, 2007, 79, 1349-1355.
105. S.I. Lysenko, B.A. Snopok, V.A. Sterligov, E.V. Kostyukevich and Yu.M. Shirshov, Optics and Spectroscopy, 2001, 90 (4), 606-616.
106. M.V. Riquelme, H. Zhao, V. Srinivasaraghavan, A. Pruden, P. Vikesland and M. Agah, Sensing and Bio-Sensing Research, 2016, 8, 47-54.
107. J. Y. Lichtenberg, Y. Ling, S. Kim, Sensors (Basel, Switzerland), 2019, 19(11), 2488.
108. N.C.H. Le, V. Gubala, R.P. Gandhiraman, S. Daniels and D.E. Williams, Langmuir, 2011, 27 (14), 9043-9051.
109. P. Boltovets, S. Shinkaruk, C. Bennetau-Pelissero, B. Bennetau and B. Snopok, Talanta, 2011, 84 (3), 867-873.
110. Snopok and I. Kruglenko, The Analyst, 2015, 140, 3225-3232.

111. I.V. Kruglenko and B.A. Snopok, Theoretical and Experimental Chemistry, 2018, 54 (1), 53-60.
112. O. Kvítek, J. Siegel, V. Hnatowicz and V. Švorčík, Journal of Nanomaterials, 2013, Article ID 743684, 15 pages.
113. K.M. McPeak, S.V. Jayanti, S.J.P. Kress, S. Meyer, S. Iotti, A. Rossinelli and D.J. Norris, ACS Photonics, 2015, 2 (3), 326-333.
114. R. Malureanu and A. Lavrinenko, Nanotechnology Reviews, 2015, 4(3), 259-275.
115. V. Scherbahn, S. Nizamov and V. M. Mirsky, Toward ultrasensitive surface plasmon resonance sensors, in: M. Schoning and A. Poghosian (ed), Springer Series on Chemical Sensors and Biosensors (Methods and Applications), Springer, Berlin, Heidelberg, 2018, pp.409-448.